Journal of Structural Geology 210 (2026) 105759

Contents lists available at ScienceDirect

Journal of Structural Geology

journal homepage: www.elsevier.com/locate/jsg

Pluton-emplacement-related fracturing in the thermometamorphic marble of Campiglia Marittima (Northern Apennines)

G. Risaliti [a,*], R.E. Rizzo [b,c], S. Tavani [a], C. Montemagni [a], M. Coli [a], P. Vannucchi [a]

[a] Dipartimento di Scienze della Terra, Università degli Studi di Firenze, Via G. La Pira, 4, Firenze, 50121, Italy
[b] Department of Earth Sciences, Utrecht University, Princetonlaan 8a, 3584 CB Utrecht, the Netherlands
[c] School of GeoSciences, University of Edinburgh, The King's Buildings, James Hutton Road, Edinburgh, Scotland, EH9 3FE, United Kingdom

ARTICLE INFO

Keywords:
Fracture
Marble
Brittle deformation
Pluton emplacement
Structural analysis

ABSTRACT

Motivated by the paucity of studies on fracture networks in thermally metamorphosed rocks, in this paper we present and analyse the fracture pattern within the Campiglia Marittima Marble. It is a thermo-metamorphic rock formed during the Neogene emplacement of a granitic pluton in western Tuscany (Italy), in the inner portion of the Northern Apennines thrust belt, affected by post-orogenic back-arc extension. To obtain data from inaccessible outcrops, increase the number of measurements, and capture fracture characteristics at multiple scales, we integrated fracture digitization on 3D Virtual Outcrop Models with the traditional field mapping. Our results show that the fractures on the cap rock around the top of the pluton are clustered into radial and concentric patterns. Furthermore, in the whole metamorphic aureole, fractures cut metamorphic features, such as folds or schistosity, confirming that brittle deformation postdates the metamorphic event. Away from the pluton emergence, the orientation of fractures aligns with regional-scale extensional trends. Therefore, we interpret the fracture distribution as due to the pluton rise, which acted as a "localised" stress source during its ascent, deforming the already cooled marble under brittle conditions.

1. Introduction

The study of fracture attributes (i.e., length, orientation, clustering, and connectivity) within rock masses is a central topic in structural geology, and has attracted extensive research over the last decades. Fractures are a key feature for interpreting stress evolution in geological processes (Hancock, 1985; Pollard and Aydin, 1988; Hancock and Engelder, 1989; Cosgrove and Hudson, 2016), and for understanding changes in rock mass rheology (Byerlee, 1978; Mancktelow, 2009; Yue et al., 2024). Moreover, fracture networks are fundamental to a wide range of geological processes and industrial applications, including fluid circulation, mineralization, geothermal systems, hydrocarbon production, and energy storage (e.g., Aguilera, 1998; Berkowitz, 2002; Bratton et al., 2006; Spence et al., 2014; Brogi et al., 2016; Cosgrove and Hudson, 2016; Lavenu and Lamarche, 2018; Tóth et al., 2022). Their characterisation is also critical in extractive sectors such as quarrying (Cosgrove and Hudson, 2016).

The development of fracture networks has been extensively studied (Hancock, 1985; Peacock et al., 2018), both across various geological (Segall and Pollard, 1983; Hancock and Engelder, 1989; Lavenu et al., 2013; Tavani et al., 2015) and mechanical contexts (Segall, 1984; Narr and Suppe, 1991; Bai and Pollard, 2000; Lamarche et al., 2012).

In particular, the characterisation of fracture networks is central for high-enthalpy geothermal systems forming in magma-rich rifted margins. In these environments, fracture networks above rising plutons record the interplay of two distinct processes: (i) a regional extension, with a far-field stress remaining relatively constant (despite local rotations and heterogeneities related to fault propagation and linkage), and (ii) a "localised" nearly-vertical push induced by the intruding plutonic body (Odé, 1957; Koide and Bhattacharji, 1975; Muller and Pollard, 1977; Chadwick Jr and Dieterich, 1995; Vigneresse et al., 1999; Walter et al., 2013; Acocella, 2021, and references therein).

However, the intrusion not only progressively modifies the net stress field, but also alters the rheology of the system, triggering thermo-mechanical modifications of the host rock (Morgan, 1998). This process can eventually lead to the annealing and obliteration of pre-existing

This article is part of a special issue entitled: A tribute to Juliette Lamarche published in Journal of Structural Geology.

* Corresponding author.
E-mail addresses: giacomo.risaliti@unifi.it (G. Risaliti), r.e.rizzo@uu.nl (R.E. Rizzo), stefano.tavani@unifi.it (S. Tavani), chiara.montemagni@unifi.it (C. Montemagni), massimo.coli@unifi.it (M. Coli), paola.vannucchi@unifi.it (P. Vannucchi).

https://doi.org/10.1016/j.jsg.2026.105759
Received 6 April 2026; Received in revised form 11 June 2026; Accepted 17 June 2026
Available online 20 June 2026

fracture networks (Passchier and Trouw, 2005; Gratier and Gueydan, 2007). Consequently, the study of fracture networks within thermometamorphic rocks becomes particularly valuable, as they primarily record the final stages of pluton emplacement. This effectively eliminates the complexity of decoupling pluton-induced fractures from pre-existing structural inheritance, a common issue when the host rock lacks a complete thermo-metamorphic reset.

Here we report on the fracture pattern affecting the thermometamorphic Campiglia Marittima Marble, located in western Tuscany (Italy). The Campiglia Marittima Marble formed during Messinian emplacement of a granitic pluton at a shallow crustal level (3-4 km depth); following the main orogenic event responsible for the formation of the Northern Apennine fold-and-thrust belt (Giannini, 1955).

The Campiglia Marittima Marble thus provides a useful analogue for studying pluton-related geothermal reservoirs, such as those present in Tuscany (Cataldi et al., 1978; Brogi et al., 2016; Peccerillo, 2017; Liotta et al., 2021). Furthermore, evaluating the Campiglia Marittima Marble rock mass can be useful for quarrying purposes (Bandini and Berry, 2013; Risaliti et al., 2026).

A detailed characterisation of the fracture patterns within the Campiglia Marittima Marble constrains the geological processes governing brittle deformation in thermally metamorphosed marbles and has direct implications for practical applications, such as identifying primary fluid pathways and defining rock mass parameters for marble exploitation. This case study is particularly advantageous compared to other examples in the Northern Apennines, due to the extensive exposure of the outcropping host rock around the intrusive igneous body. Furthermore, the presence of a competent host rock such as marble simplifies the analysis of brittle deformation, whereas in softer lithologies it would be more challenging.

We integrated traditional field surveys with digital analysis on 3D Virtual Outcrop Models (VOMs). As a result, we establish a clear picture of fracture evolution near the pluton and use them as a stress field indicator, providing both information about the geological processes that affected the area and data that can be used for practical applications.

2. Geology of Campiglia Marittima mountains

The studied area is located in central-western Tuscany, within the inner sector of the Northern Apennine fold-and-thrust belt (Boccaletti et al., 1980; Molli, 2008; Conti et al., 2020, Fig. 1a). The Apennines, together with the Tyrrhenian Sea, form a coupled thrust-belt back-arc basin, developed due to the eastward retreat of the subduction zone along which the Alpine Tethys and the Adria passive margin have been subducted underneath Europe (Malinverno and Ryan, 1986; Jolivet et al., 1999). In detail, central-western Tuscany has been affected by nappe stacking during the Cenozoic until active compression migrated to the frontal (NE) part of the belt and back-arc extension overprinted compressional structures. Extensional tectonics affected western Tuscany since the middle/late Miocene, leading to the disarticulation of the thrust pile and the development of horst and graben structures bounded by NW-SE to N-S striking extensional faults (Carmignani et al., 1994; Brogi and Liotta, 2008; Barchi, 2010). Slightly post-dating the onset of extensional tectonics, partial crustal melting and associated pluton emplacement and volcanism occurred during back-arc rifting in western Tuscany. The Mt. Capanne and Gavorrano plutons, dated at 7.0-7.3 Ma (Barboni et al., 2015) and 4.4 Ma (Serri et al., 2001), respectively, are examples of this. This interpretation of western Tuscany as a classical magma-rich rift setting has been challenged by some authors, who inferred a pulse of late Miocene contraction during back-arc opening (e.g., Bonini et al., 2014).

The Campiglia Marittima mountains are part of this volcano-tectonic framework. They consist of a ~10 km long, ~4 km wide horst delimited by a N-S to NNE-SSW trending normal fault on its western side, and by a set of NNW-SSE to NW-SE trending normal faults on its eastern side. The structure terminates to the south with a set of transverse NE-SW trending faults (Giannini, 1955; Costantini et al., 1993; Acocella et al., 2000, Fig. 1b and c). The horst is cored by the late Miocene *Botro ai Marmi* granitic pluton, surrounded by an aureole of thermo-metamorphism affecting Triassic and Early Jurassic shallow-water carbonates.

The area around Campiglia Marittima Mts. exposes the following tectonic stack, from bottom ro top.

- Tuscan Units: Triassic to Early Jurassic shallow-water carbonates, Jurassic to Oligocene basinal limestones, marls, shales, and Oligocene to early Miocene sandstones;
- Subligurian Units: middle Eocene to early Miocene deep-water shales, marls, and limestones (middle Eocene – early Miocene);
- Ligurian Units: Late Cretaceous to middle Eocene deep-water shales, marls, marly limestones, and limestones;

These units were stacked during the Late Cretaceous – Early Miocene Alpine–Apennine orogeny (Costantini et al., 1993; Cerrina Feroni et al., 2007a, 2007b; Molli, 2008; Conti et al., 2020). Afterwards, the following units were deposited/emplaced.

- Neogene Autochthonous Units: post-orogenic Pleistocene sand and silt;
- Magmatic Complex Units: *Botro ai Marmi* Granite Fm., Porphyry Dikes Fm., and San Vincenzo Rhyolite Fm. (late Miocene – early Pliocene; Fig. 1b and c; Giannini, 1955; Barberi et al., 1967; Costantini et al., 1993; Peccerillo, 2017; Di Vincenzo et al., 2022).

The horst of Campiglia Marittima is mainly composed of the lowermost formations of the Tuscan Units, predominantly the Rhaetavicula Contorta Limestone Fm. (Late Triassic) and the Calcare Massiccio Fm. (Early Jurassic; Fig. 1b and c).

Relevant to this study, at the end of the Messinian, the emplacement of the *Botro ai Marmi* granitic pluton at a shallow crustal level (3–4 km depth, 1–1.5 Kbar pressure; Leoni and Tamponi, 1991) caused the metamorphism of the Triassic Rhaetavicula Contorta Limestone and the early Jurassic Calcare Massiccio formations. Hereafter, the marble derived from the Calcare Massiccio Fm. protolith is referred to as the "White Marble" and the marble from the Rhaetavicula Contorta Limestone Fm. protolith as "Grey Marble".

Pluton emplacement induced a schistosity within the metamorphosed units, which is often visible at the outcrop scale and is subparallel to the original bedding (Acocella et al., 2000; Vezzoni et al., 2018; Papeschi et al., 2025). As a syn-pluton emplacement deformation feature, in this work, the orientation of the schistosity is treated as a reference for the fracture network, i.e., as an equivalent of the bedding in fractured carbonates. At the macroscopic scale, both the metamorphic and non-metamorphic limestone are folded into a N-S oriented antiform (Fig. 1b and c). The N-S elongated shape of the metamorphic aureole reflects the underlying N-S elongated shape of the granite (Acquater, 1994; Vezzoni et al., 2018; Papeschi et al., 2025). The metamorphic aureole boundary is truncated on the west by the main N-S trending fault that defines the horst, while it decreases gradually on the remaining sides (Fig. 1b and c). The thickness of the metamorphic aureole ranges from 400 to 500 m (Papeschi et al., 2025). The top of the pluton, which is also the only exposed portion of the Botro ai Marmi granite, is situated in the central-southern sector of the aureole (Fig. 1b).

Lithologically, the Campiglia Marittima Marble is a nearly pure marble, with the White type being particularly pure. It is primarily composed of calcite crystals (95% to 99%), with dolomite occasionally present in the Grey Marble (rarely up to 7-10%). Accessory primary minerals randomly distributed within the marble (we are not considering mineralogy of localized skarn deposits or igneous rocks) include phlogopite, tremolite, diopside, and K-feldspar (Leoni and Tamponi, 1991; Franzini et al., 2010; Papeschi et al., 2025). The Campiglia Marittima Marble is characterized by a strong to weak schistosity and a predominantly heteroblastic fabric, with homeoblastic marble

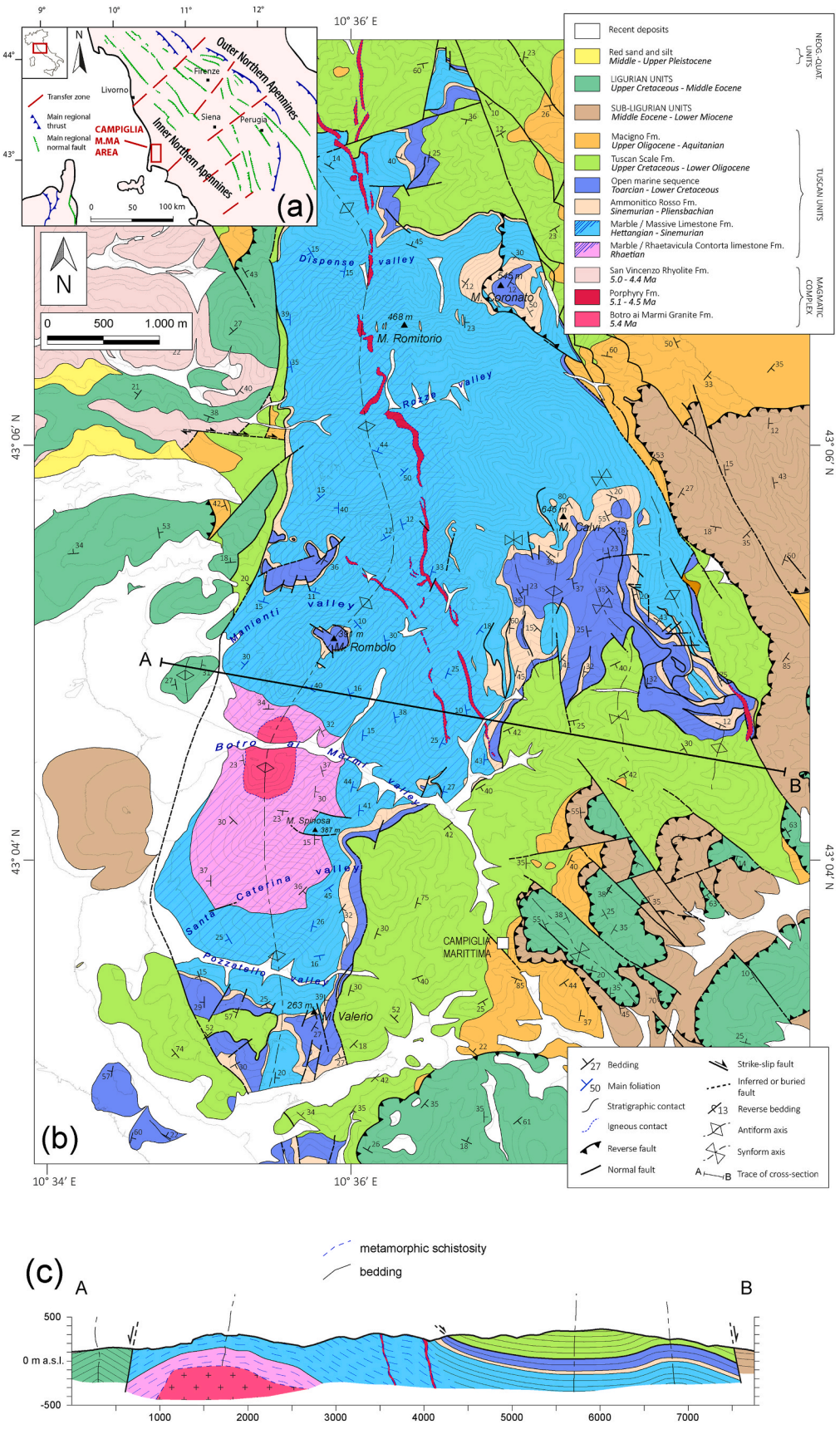

Fig. 1. (a) Location of the study area within the Northern Apennines; (b) geological map of the Campiglia Marittima ridge, with (c) the corresponding geological cross-section (modified after Cerrina Feroni et al., 2007a, 2007b; Papeschi et al., 2025). Topographic contour lines are spaced at 25 m intervals.

developing occasionally. The schistosity is defined by a shape-preferred orientation (Passchier and Trouw, 2005) of calcite crystals (Cavari et al., 2012; Bandini and Berry, 2013; Papeschi et al., 2025).

Marble grain size decreases with distance from the pluton contact, ranging from a few millimetres within the inner part of the aureole (tens of meters from the contact) to approximately 20-50 μm in the external parts (400-500 m; Franzini et al., 2010; Cavari et al., 2012; Lezzerini et al., 2021; Papeschi et al., 2025).

3. Methods

We collected fracture data at 44 structural stations across the metamorphic area exposing the marble. At each station, we recorded fracture attributes, including orientation (dip direction and dip), cross-cutting relationships, and spacing of the main sets. Because of limitations due to outcrop conditions, we decided to measure fracture properties directly on the outcrop, without using scanlines or scanwindows. To supplement field data collection as well as to reach inaccessible outcrops, an Unmanned Aerial Vehicle (UAV) was used to acquire outcrop photos for the reconstruction of 3D VOMs via photogrammetry. We employed a DJI Mini 3 Pro, capturing 9 MP, approximately 4 Mb size photos. We acquired a total of 515 images. Images were processed using the PIX4Dmapper software (Pix4D, 2025) via the standard Structure from Motion - Multiview Stereo workflow (photo alignment → tie points → point cloud → mesh → texture; further details are provided in the Supplementary Material, Table A). We registered the models via direct georeferencing, using Global Navigation Satellite System/Inertial Measurement Unit positional data embedded into image metadata. While relative accuracy of VOM orientation and scaling using UAV coordinates is usually reliable for structural analysis purposes, the absolute accuracy of VOM positioning can sometimes lead to offset errors (Menegoni et al., 2019). However, we checked the VOM positioning manually. B Fractures on VOMs were manually digitised using the OpenPlot software (Tavani et al., 2011). The geometric orientation uncertainty propagated into the analysis is estimated to be consistent with compass measurement errors (ca. 3°; Menegoni et al., 2019). A minor truncation bias exists for fractures smaller than the model's pixel resolution (on average less than 3 cm). However, fractures extracted from VOMs were used only to provide orientation data. Further details on VOM properties and photos are provided in the Supplementary Material (Table B).

We grouped the data into sets based on consistency of clustering, field evidence, and cross-cutting relationships. We compared fracture orientations with the attitude of the main schistosity (where visible). We plotted fracture orientations using Stereonet11 (Cardozo and Allmendinger, 2013). Details about stereographic projections and contouring are reported in the figure captions.

We used the FracPaQ2D MATLAB™ Toolbox (Healy et al., 2017) to analyse 2D orthophotos extracted from selected VOMs. Orthophotos ranged from 8 m to 20 m per side; fracture traces were manually digitised in Adobe Illustrator (2023) (Adobe Inc.), at a consistent zoom level for each orthophoto, and then imported into FracPaQ2D. The number of segments used for each fracture trace depends on trace length and straightness; on average, we used between 1 and 10 segments per trace. We applied Maximum Likelihood Estimators (MLE) to fracture length data extracted from the whole orthophotos to identify the best-fitting fracture length distribution (Rizzo et al., 2017), and used smaller representative squares to estimate fracture density (P20) and intensity (P21) (Dershowitz and Einstein, 1988; Dershowitz and Herda, 1992, Figs. 6 and 9).

4. Results

4.1. Survey of the area and fracture detection

We collected a total of 864 fracture measurements within the metamorphic aureole, employing a hybrid method that combined field mapping (29 sites, 509 data) with digital mapping using VOMs via photogrammetry (14 sites, 355 data; Fig. 2). Data were primarily collected from the White Marble (39 sites), with a smaller subset in the Grey Marble (5 sites). Observed discontinuities are mainly open fractures. Rare veins, filled with red clay or, near igneous outcrops, quartz, calcite, or skarn, were also observed. Critically, we identified no significant faults (i.e., displacement >5 m) within the metamorphic aureole and excluded them from this study. The structural station locations and fracture distribution are detailed in Fig. 2. The highest data density was achieved in the Mount Rombolo area (between the Manienti and Botro ai Marmi valleys; Fig. 1b and 2).

At the outcrop scale, the fracture network is systematically characterised by the occurrence of two sets oriented at high angles to each other, which include steeply dipping fractures (typically >70°, with occasional dips of 60°) (Fig. 2). The frequent cross-cutting relationships between the two sets suggest they are largely coeval.

Throughout the entire metamorphic aureole, fractures constantly cut the main marble schistosity. However, occasionally, slightly inclined and open fractures have preferentially exploited the schistosity planes, suggesting the schistosity acts as a mechanically weak layer. In these cases, other fracture sets are observed to either cut or terminate against these schistosity-parallel discontinuities (Fig. 2).

4.1.1. Fracture orientation with respect to the pluton top

Observed fracture sets apparently do not show a clear and unambiguous relationship with a regional trend or with the major structures affecting the Campiglia horst (Fig. 2). Nevertheless, the presence of two, almost vertical and orthogonal sets, which always predate other sets (if present), has been observed throughout the entire metamorphic aureole (Figs. 2 and 6).

We grouped data in two different areas, based on distance from the Botro ai Marmi Pluton top and the orientation of the main fracture sets:a first area defined by a buffer of ~1 km from the pluton contact, between the Manienti Valley (North) and Santa Caterina Valley (South), and a second area comprising the rest of the metamorphic aureole (Fig. 1b and 3).

In the external domain, near the western boundary of the metamorphic aureole (which is delimited by a W-dipping normal fault), the dominant sets trend N0°–N40° and N70°–N135°, both steeply inclined (Fig. 3a). These sets occur along the entire western side of the aureole, even considering the stations within this area individually (Figs. 2 and 3a). Moving toward the eastern side of the metamorphic aureole, fracture orientations become more distributed, mainly striking around N5°, N45°, N100° and N150° (Fig. 3a).

In the internal domain, fractures do not show geometrical linking with the faults bordering the horst, or the main antiform characterising the metamorphic aureole (Fig. 2). Instead, if we consider the structural stations' position (hence, data position) with respect to the exposed pluton top, the two main orthogonal fracture sets align along a radial and a concentric strike, centered on the pluton top itself (Fig. 3b). The presence of a concentric component perturbing the metamorphic aureole is suggested also by the trend of the innermost Porphyry Dike, known as the "Coquand" dike (Fig. 1b and 3b). This dike is almost vertical (Vezzoni et al., 2016, 2018), and describes the top-right side of a slightly prolate ellipsoid centered on the *Botro ai Marmi* pluton top, with a major axis trending around N23° (Fig. 1b and 3b).

The presence of a radial and concentric fracture pattern is distinguishable (and comparable) from a regional one by plotting on a Cartesian system the fracture strike (Y axis) against its geographic angular position (X axis) with respect to an established center (in our case, the pluton top), which must also be the center of the radial and concentric pattern too (Quintà et al., 2012, Fig. 3c). In a regional fracture pattern, fracture strike is approximately constant and does not vary with position; in a fully radial and concentric pattern, fracture strike follows lines with 45° angular coefficient, separated by 90° of angular position (Fig. 3c). Mixed patterns are also possible, plotting along intermediate

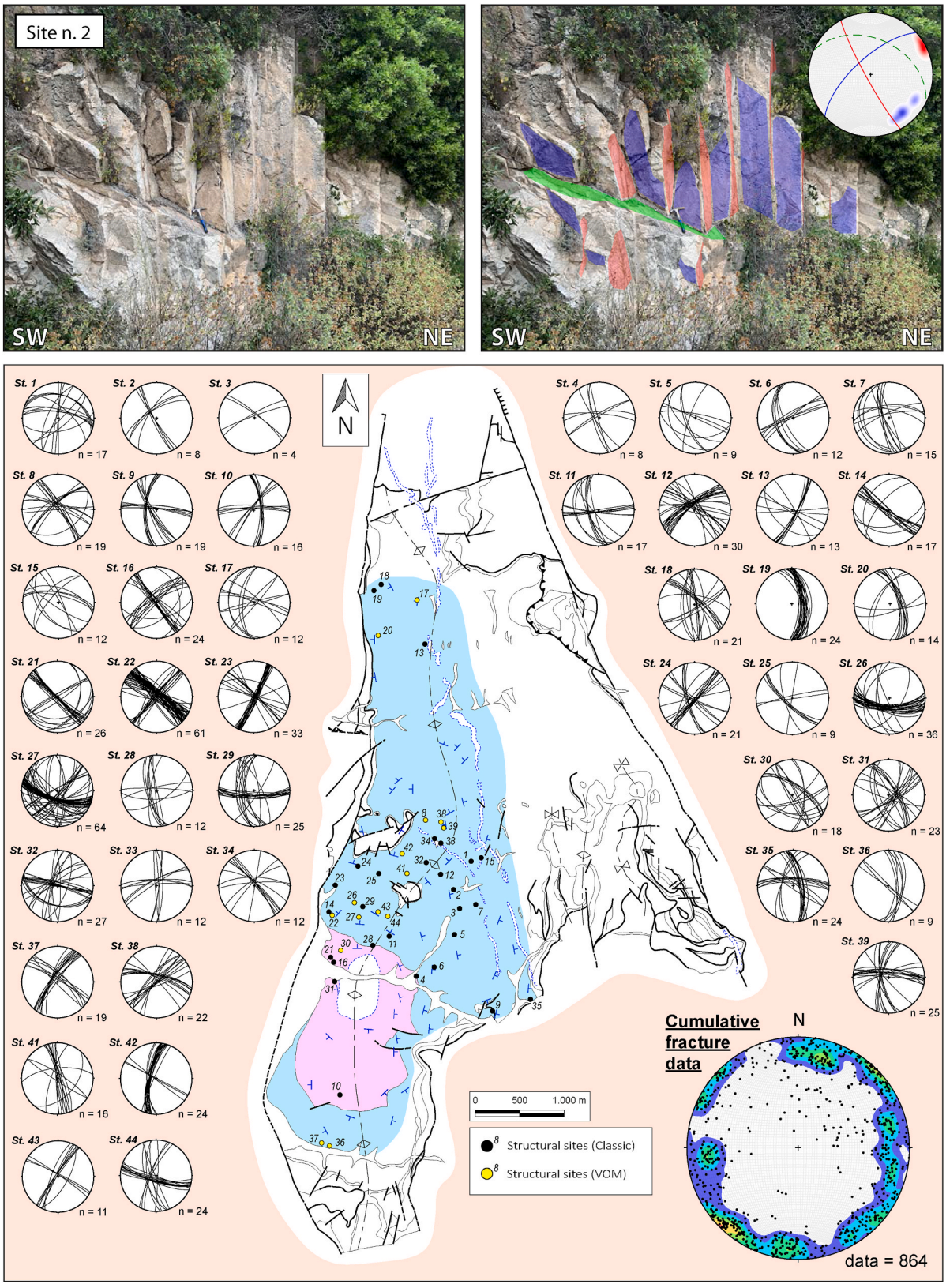

Fig. 2. Structural map of the Campiglia Marittima *horst*, with the location of structural sites and fracture distribution (plots). The coloured part evidence the metamorphic aureole. Refer to the legend of Fig. 1 for geological formations and types of geological contact. On top, example of site n. 2; red and blue great circles represent fracture sets, while green dashed circle is the main schistosity. All stereographic projections are calculated on a lower-hemisphere equal-area projection; pole density contour of cumulative fracture data in was generated using a smoothed 1% area counting circle. (For interpretation of the references to colour in this figure legend, the reader is referred to the Web version of this article.)

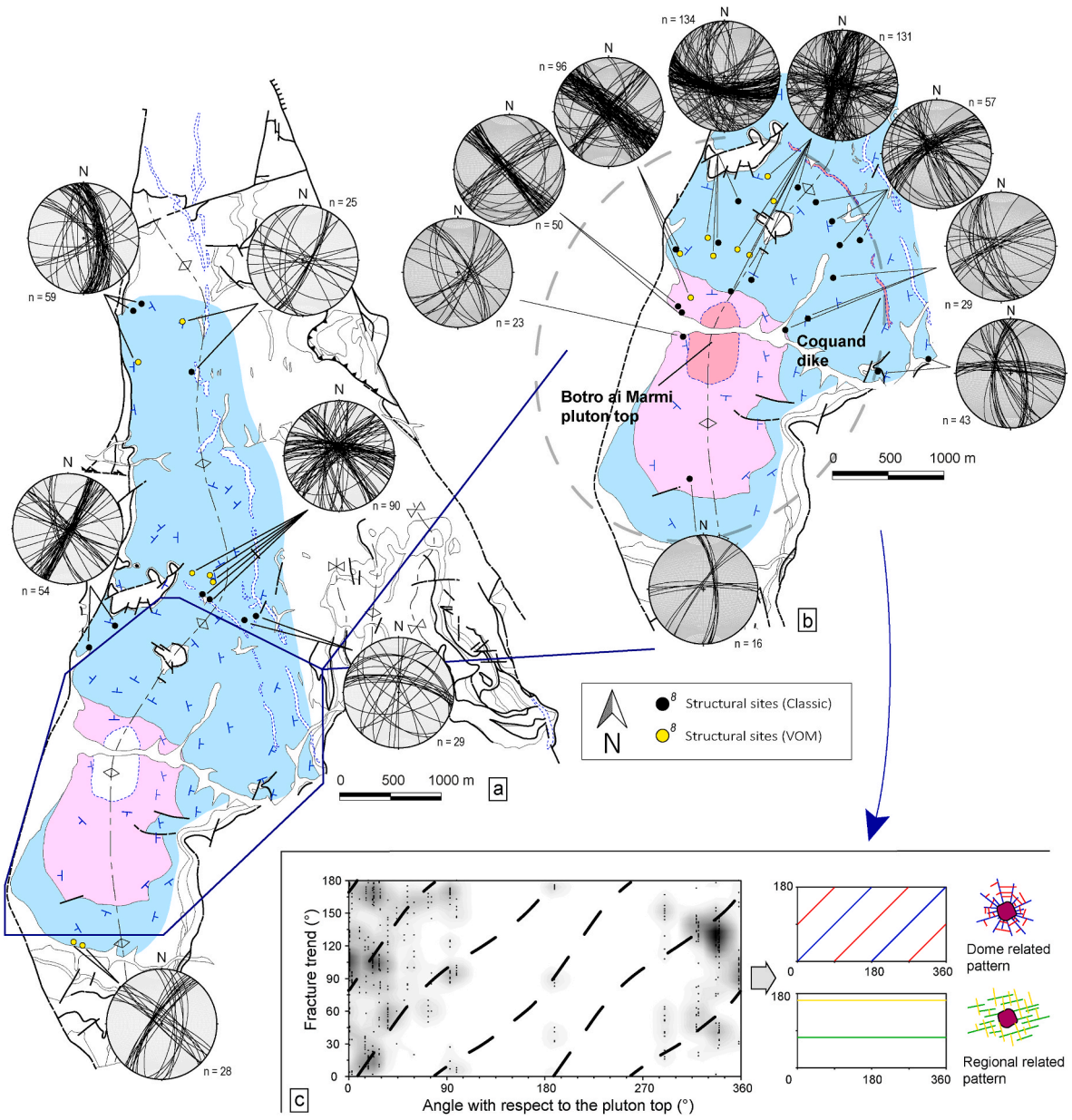

Fig. 3. (a) Structural map of the Campiglia Marittima *horst*, with location of structural sites and related cumulative fracture plots (lower-hemisphere, equal-area projection). See Fig. 1 for related positioning; refer to the legend of Fig. 1 for geological formations and types of geological contact. (b) Focus of the Botro ai Marmi pluton top "area of influence" within the blue insert in (a). Cumulative plots denote the radial and concentric sets with respect to the pluton top. Details of pluton top and Coquand Porphyry Dike are reported. The dark dashed line represents the ellipsoidal shape based on Coquand dike orientation. (c) On the left, diagram with fracture trend (strike, Y axis) against the angular position with respect to the pluton top (X axis); point data (n = 578) with related contour represent actual fracture orientations from the pluton-top related area (b), while dashed lines represent hypothesized distribution from an ellipsoidal radial and concentric pattern based on the Coquand Dike trend (drawn with dark dashed line in (b)). Data contour was generated using a 2D Kernel density estimation (Gaussian Kernel). On the right, two end-member examples of the same diagram for dome related and regional related patterns (modified after Quintà et al., 2012). See text for further details. (For interpretation of the references to colour in this figure legend, the reader is referred to the Web version of this article.)

and curvilinear distributions (Quintà et al., 2012).

We plotted fracture strike from the area around the *Botro ai Marmi* pluton top against the angular position relative to the pluton top (Fig. 3c), and calculated the expected distribution of hypothetical radial and concentric fracture orientations within an ellipsoid matching that described by the Coquand Dike; these are shown alongside fracture data contours (Fig. 3c). The fracture data align with the ellipsoidal dike distribution (Fig. 3c).

4.1.2. Spacing analysis

Spacing data were collected perpendicular to the fracture sets; therefore, we did not apply any correction to avoid sampling orientation bias (Terzaghi, 1965). We estimated a mean spacing value for all cumulative fracture sets of 0.22 m within White Marble and 0.33 m within Grey Marble respectively (Fig. 4). However, these values show a high standard deviation across all measurements, which is greater for the Grey Marble (Fig. 4).

We further divided spacing values within the pluton top area of influence. We calculated a mean spacing value for the radial and concentric sets of 0.20 m and 0.23 m within White Marble (Fig. 4), respectively. These values are notably higher within Grey Marble, at 0.33 m and 0.36 m, respectively (Fig. 4). Again, the derived values show

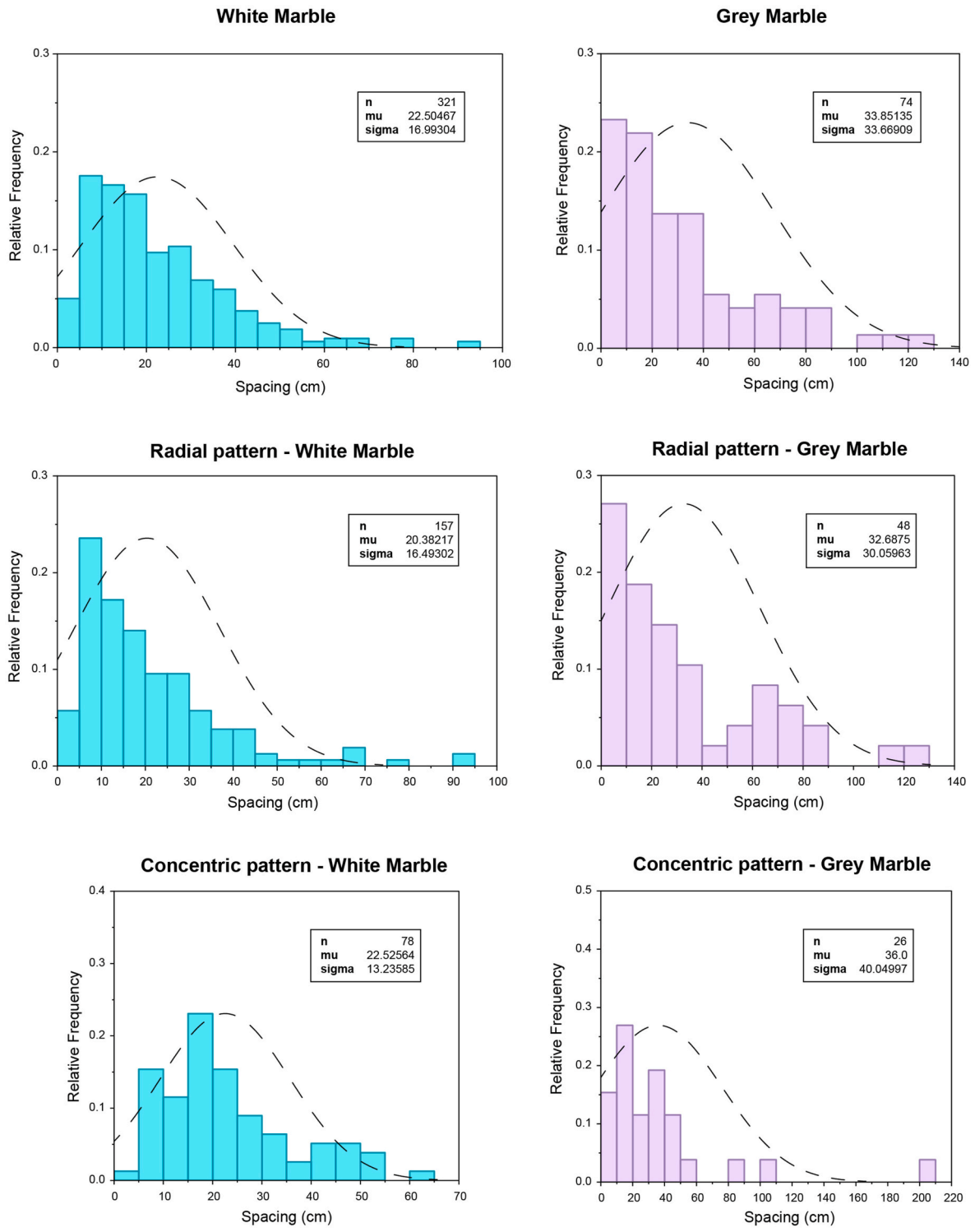

Fig. 4. Fractures spacing values within White Marble (left) and Grey Marble (right), with relative log-normal distribution. Total data (top); radial (middle) and concentric (bottom) fracture patterns. Radial and concentric sets data are referred to the pluton top-fracture related area.

a high standard deviation across all measurements, although consistently greater for the Grey Marble (Fig. 4). Furthermore, spacing values for both sets exhibit a general trend with distance from the pluton: a decrease within the first 700-1000 m is followed by a slight increase after ~1.5 km (Fig. 5). This trend is consistent for both radial and concentric fracture sets, though the radial set shows greater local variability (Fig. 5).

4.2. *Analysis with FracPaQ2D*

We used FracPaQ to analyse the fracture lineaments extracted from orthophotos (as vertical sections) in three specific sites: no. 17 ("Calasorbi Quarry"), no. 20 ("Broccatello Quarry"), and no. 27 ("Pari Quarry"), (Fig. 6). We selected these sites for two reasons: first, they are the only locations where it is possible to access reasonably large, planar exposures suitable for mapping fracture traces; second, they are located

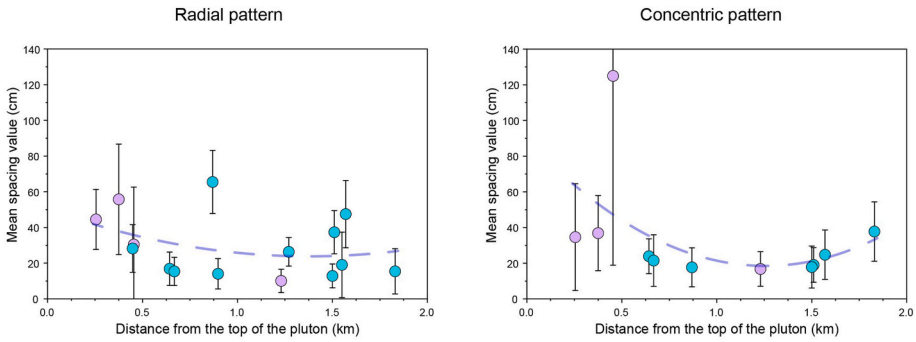

Fig. 5. Spacing values of radial (left) and concentric (right) fracture patterns against with distance from Botro ai Marmi pluton top. Single dots are referred to as the mean value per each site, where their colour is referred to the lithology (cyan for white marble and violet for grey marble). Black vertical lines represent standard deviation, and blue dashed lines are trend lines. (For interpretation of the references to colour in this figure legend, the reader is referred to the Web version of this article.)

both within the pluton-top-related area (Site no. 27) and the external part (Sites nos. 17 and 20). Specifically, Calasorbi quarry and Pari quarry trend NNE–SSW and face WNW, while Broccatello quarry trends W–E and faces south (Fig. 6). Map dimensions are approximately 12.5 × 10.0 m for Broccatello quarry, 14.0 × 12.0 m for Calasorbi quarry and 18.0 × 17.0 m for Pari quarry. The square maps we used for density and intensity calculations measure approximately 7.0–8.0 m per side for all sites (Figs. 6 and 9). Fig. 6 (middle column) shows a brief summary of traces and segments length, and the number of nodes obtained from line-drawings used as input for FracPaQ2D.

4.2.1. Fracture traces analysis

Vertical to steeply inclined fractures constitute the most abundant features detected at all sites; these are followed by less inclined (35° to 65°), oblique fractures and slightly inclined, in places nearly horizontal discontinuities opened exploiting the main schistosity planes (Fig. 6). The schistosity-parallel discontinuities are more abundant at the Calasorbi quarry compared to the other sites (Fig. 6). Trace lengths at all sites show an inverse order: the discontinuities opened along the main schistosity are the longest structures, followed by oblique fractures and nearly vertical ones (Fig. 7). The first two sets, in places, reach several metres in length (around 4.0-4.5 m in Broccatello quarry and Pari quarry, and almost 6.0 m in Calasorbi quarry); however, the majority of detected fractures have lengths ranging between 0.5 and 1.5 m (Figs. 7 and 8).

We performed a fracture trace length analysis, including all sites, to determine their underlying statistical distribution. For this analysis we used Maximum Likelihood Estimators (Rizzo et al., 2017, Fig. 8) to estimate the best-fitting statistical distribution among power-law, log-normal and exponential functions; for power-law Maximum Likelihood Estimators, we considered a lower and upper cut-off of 5%. Results show that the best-fitting distribution for fracture lengths is a lognormal distribution (P = 91.52%) (Fig. 8), while power-law and exponential show a worse fit. For density (P20) and intensity (P21) analyses, FracPaQ divides maps into equal-radius scan circles. We instructed the software to use 12 circles per side within each site's square map, which resulted in circle diameters of approximately 0.6 m for all sites (Fig. 9). Scan circles maps, together with results obtained from each circle, are shown in Fig. 9, whereas values obtained for the whole maps are reported in Table 1.

Density and intensity values at the Calasorbi quarry are higher than those at Broccatello quarry, and at Pari quarry are higher than those at Calasorbi quarry. Map results show that at Pari quarry both density and intensity are more uniformly distributed compared to the other two sites (Fig. 9). Broccatello quarry and Calasorbi quarry show localized increases in fracture abundance, particularly evident in density maps (up to 50 m^{-2} within the Calasorbi quarry, left side, and 35 m^{-2} within the Broccatello quarry, central-left portion; Fig. 9).

5. Discussion

5.1. Structural summary

By subdividing the fracture data into internal and external domains relative to the pluton contact (Fig. 3), two distinct fracture patterns can be identified. The internal domain is located in the central part of the metamorphic aureole, around the Botro ai Marmi pluton top, whereas the external domain comprises the rest of the metamorphic aureole.

In the external domain, fracture orientation is coherent with that of the main faults delimiting the horst (Fig. 3a). Hence, fractures and major faults can be considered as associated with the same stress field (Hancock, 1985; Rawnsley et al., 1992; Cosgrove and Hudson, 2016).

In contrast, in the internal domain, fractures define two main sets, which are radial and concentric with respect to the Botro ai Marmi pluton top and the Coquand Porphyry Dike (Fig. 3b).

This model suggests that the Botro ai Marmi pluton emplacement may have played a key role in fracturing. Specifically, according to the difference between the internal and external domains, we define an area of influence, where the emplacement of the pluton top perturbed the regional stress field, controlling fracture orientation within a radius of approximately 2 km (Fig. 3a and b).

The observed fractures cut the schistosity throughout the entire metamorphic aureole, or they abut it in a few places where it still constitutes a physical discontinuity (Figs. 2 and 6). Thus, the fractures postdate the schistosity. Moreover, fracture dip within the pluton-related area shows no relationship with the marble schistosity attitude, and radial and concentric sets remain subvertical while increasing their distance from the *Botro ai Marmi* pluton top (Figs. 2 and 3b). Therefore, within the pluton-related area, fracture attitudes show generally no rotations, confirming that the timing of fracturing can be constrained to after schistosity formation. Fractures formed shortly after the main ductile deformation event caused by pluton emplacement, while the metamorphosed host rocks were already cooling (i.e. after the ductile-brittle transition). These geometrical relationships are further demonstrated by drawing radial and concentric cross-sections with respect to the pluton top, and projecting fracture dip and schistosity dip on them. For each cross-section, we applied a statistical analysis based on Pearson's correlation coefficient to demonstrate that no relationship exists between the variation of fracture dip and schistosity orientation (Pearson, 1895; Akoglu, 2018) The cross-sections, together with the details and results of the statistical analysis, are reported in the Supplementary Material.

5.1.1. FracPaQ analysis

FracPaQ analysis corroborates the differences in fracture nucleation inside and outside the pluton's influence zone, showing a slight increase in both density and intensity toward the pluton top (Table 1; Figs. 6 and

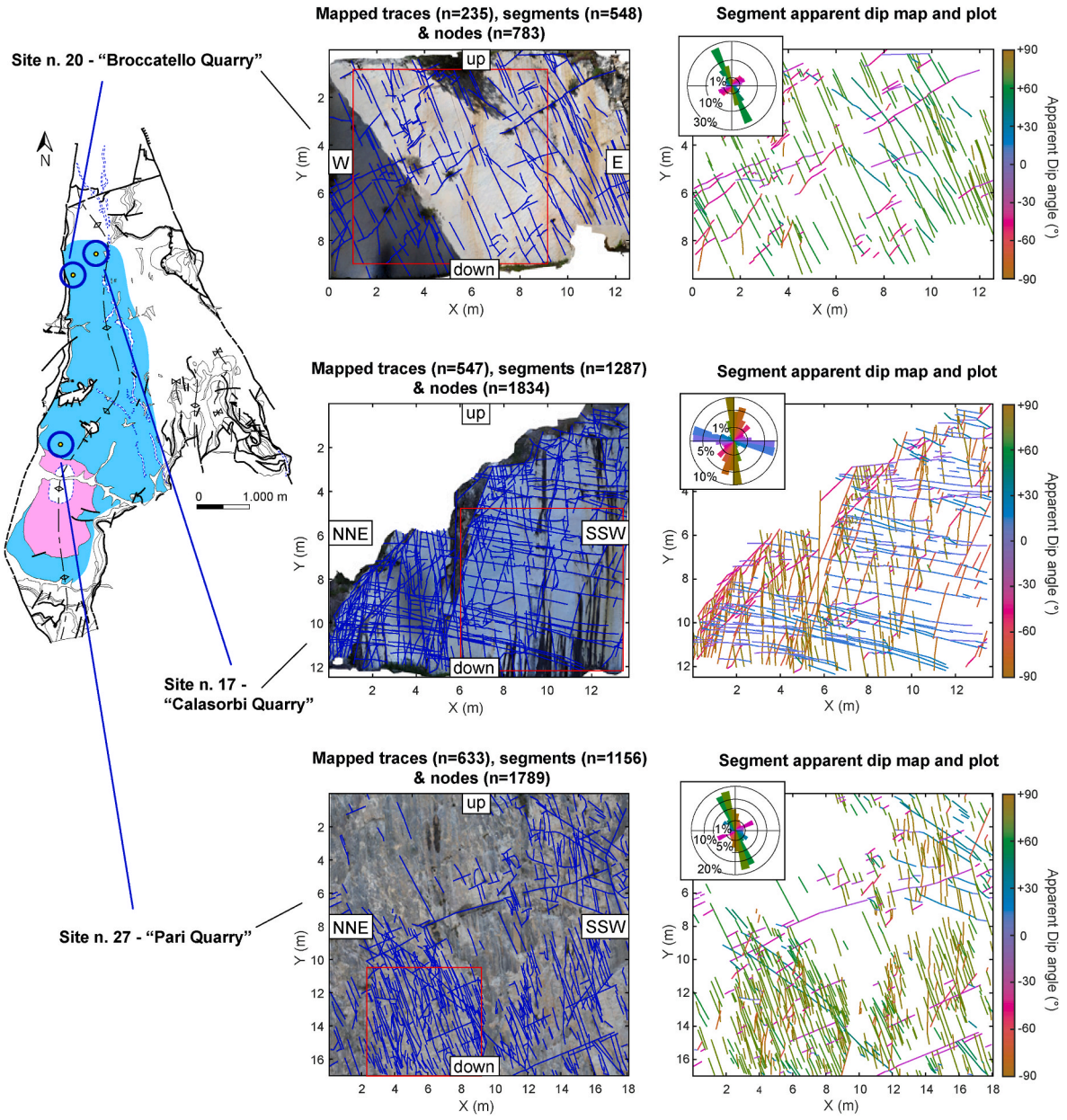

Fig. 6. (Left) Locations of sites where FracPaQ2D analyses were applied, with details of orthophotos extracted from VOMs. For geological symbols, refer to Fig. 1; for further details on orthophotos orientation, explanation in the text. Trace maps of the investigated sites (middle column) and segment strike maps with related plots (right column). Top to bottom: site no. 20, "Broccatello Quarry"; site no. 17, "Calasorbi Quarry"; site no. 27, "Pari Quarry". Orthophotos are based on vertical walls; therefore, segment strike maps and related plots have the vertical direction along the Y axis. Consequently, strike is expressed here as the apparent angle with respect to the vertical, measured counterclockwise. Red boxes within trace maps indicate areas used for density (P20) and intensity (P21) analyses (see Fig. 9). (For interpretation of the references to colour in this figure legend, the reader is referred to the Web version of this article.)

9). This suggests that under the pluton top's influence, a higher degree of brittle deformation was caused, resulting in more intense fracturing compared to that produced in the rest of the metamorphic aureole. Results obtained with Maximum Likelihood Estimators analysis on fracture traces (Fig. 8) show that a log-normal distribution is the best fit for fracture length (P = 91.52%). Such a distribution is typical of fractures in well-stratified rocks, while in this case, fracture length is inhibited by cross-cutting and terminating relationships between different sets, as well as by the limitation imposed by the natural size of the outcrops (censoring bias), which is comparable to fracture length (Bonnet et al., 2001; Cosgrove and Hudson, 2016).

5.1.2. Spacing analysis

We observed that spacing values within the pluton top area of influence are slightly higher for concentric sets compared to the radial sets (Fig. 4). These values are constantly higher in the Grey Marble than in the White Marble, although the former shows greater standard deviation (Fig. 4).

Both radial and concentric sets show a general decrease in spacing within the first 700-1000 m from the *Botro ai Marmi* pluton top (Fig. 5), followed by a slight increase beyond ~1.5 km (Fig. 5).

One explanation for the initial decrease relates to the mechanical strength differences between the Grey and White Marble lithologies, potentially due to a higher dolomite content within the Grey Marble (Schmid, 1982; Davis et al., 2008; Franzini et al., 2010), which is generally closer to the pluton. (Fig. 1b and c, 2 and **3**). However, this explanation is incomplete, as the same spacing trend persists even when considering Grey Marble and White Marble separately (Fig. 5).

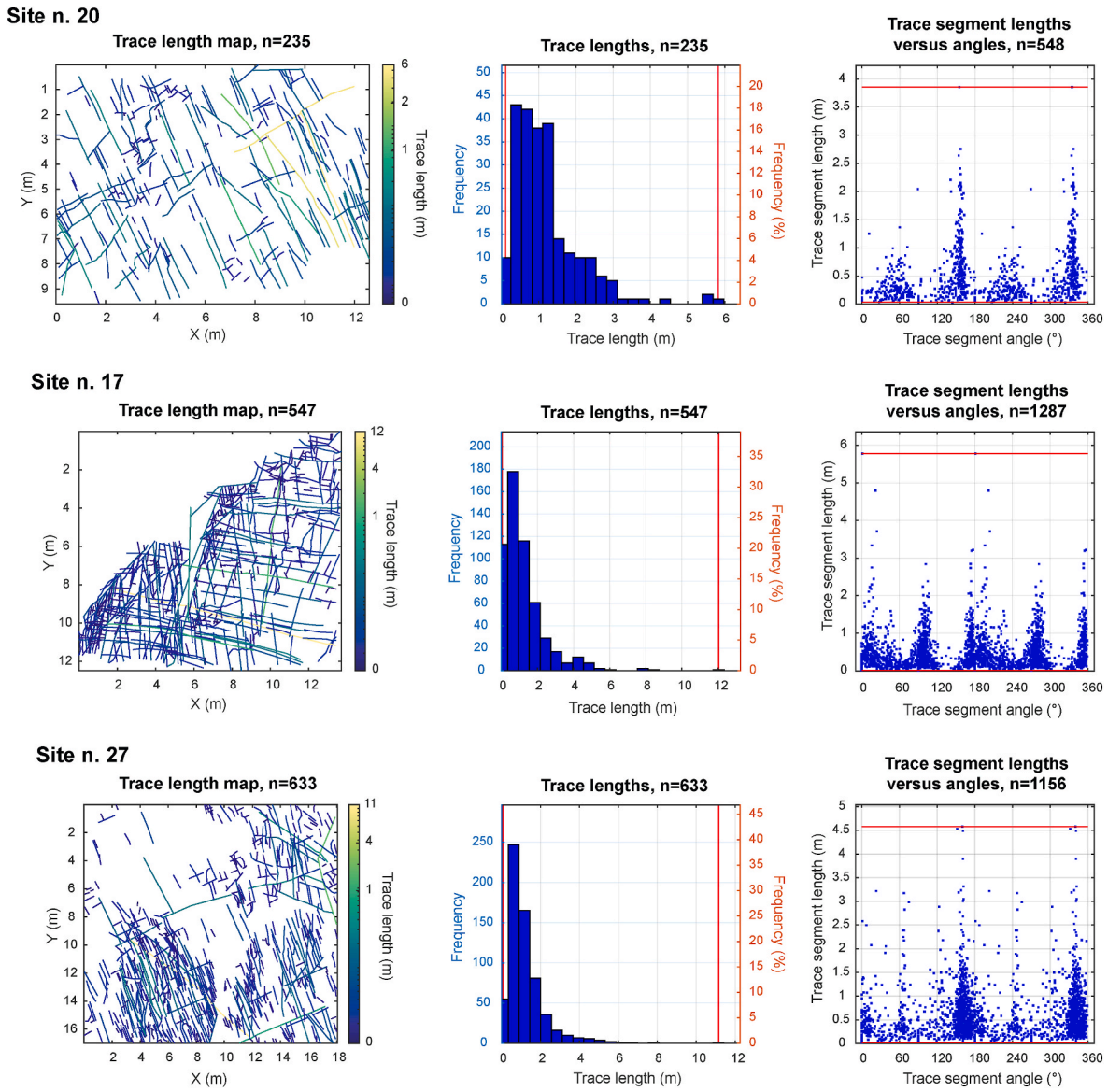

Fig. 7. Trace length maps (left column), with related frequency histograms (middle column) and plots of trace length versus angle with respect to the vertical (right column). Top to bottom: site no. 20, "Broccatello Quarry"; site no. 17, "Calasorbi Quarry"; site no. 27, "Pari Quarry".

Alternatively, grain-size variations with increasing distance from the pluton top may provide an explanation (Franzini et al., 2010; Papeschi et al., 2025). This interpretation, however, is not entirely satisfactory, as marble strength is expected to increase with decreasing grain size, which should lead to lower fracture intensity (Harbord et al., 2023). This grain-size mechanism may instead explain the behaviour observed at greater distances from the pluton top (>1.5 km), where the pluton's influence decreases.

A thermal stress effect decreasing radially from the pluton top could also be considered (Delaney et al., 1986; Martel and Bergbauer, 1997). However, this factor alone is insufficient to explain the observed initial decrease and subsequent increase in fracture spacing.Consequently, a combination of the aforementioned mechanisms should be considered. The zone characterised by the highest fracture intensity corresponds to an intermediate distance range, approximately between 700 m and 1.5 km from the pluton top.

5.2. *Proposed model and related stress field*

Previous studies have described radial and concentric structural patterns around intrusive bodies, for example, for dike emplacement episodes related to magmatic intrusions (Odé, 1957; Koide and Bhattacharji, 1975; Chadwick Jr and Dieterich, 1995; Acocella, 2021 and references therein). These studies propose and define stress-field models, showing relationships between fracture and fault formation, and their association with dike propagation, usually simultaneous with the emplacement of the magmatic body.

For example, Odé (1957) describes the relationship between local and regional stress fields based on the observation of dike propagation around a magmatic intrusion. In that case, dikes display a radial pattern around the main top of the intrusion. Moving away, they tend to be aligned along a N75° direction, imposed by the regional tectonics.

Koide and Bhattacharji (1975) study field stress imposed by magma bodies of different shapes, and their role in the development of radial and concentric brittle structures.

Acocella (2021) describes stress distribution within a conical volcanic edifice in relation to dikes emplacement. Inside the volcanic edifice, the maximum stress axis (σ_1) is subvertical, while the intermediate (σ_2) and minimum (σ_3) are respectively radial and concentric with respect to the main conduit. By moving closer to the volcano flanks, σ_1 and σ_2 tend

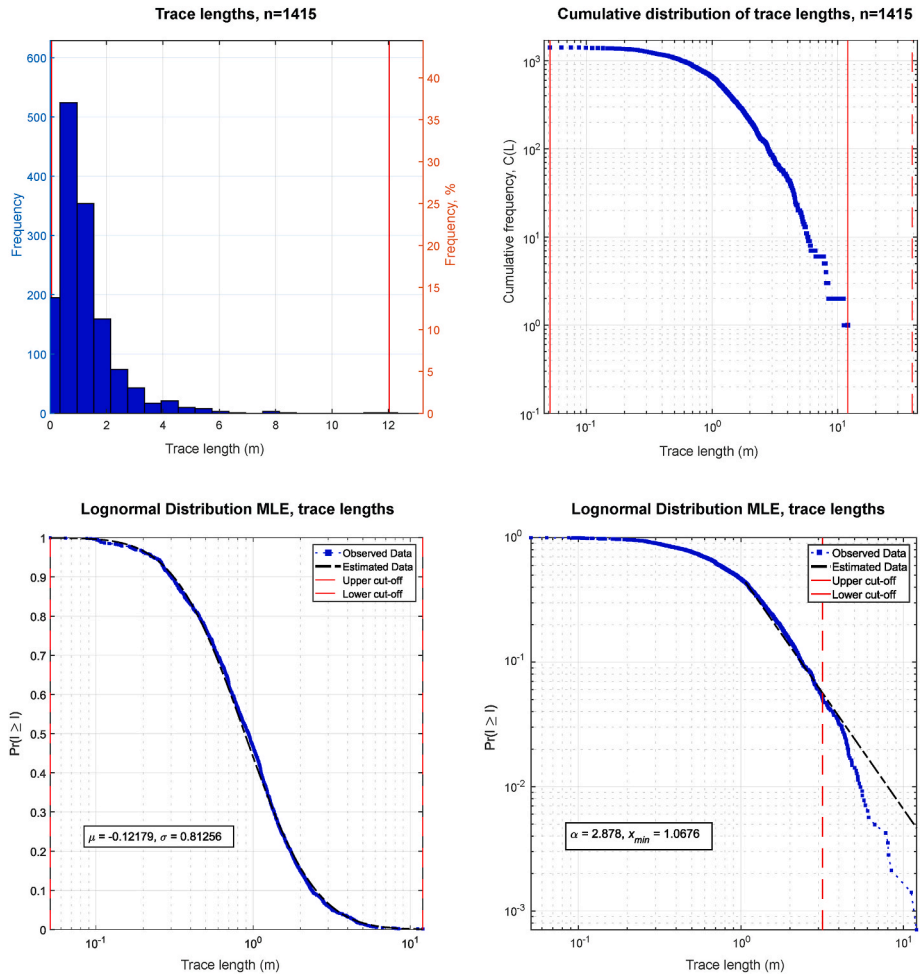

Fig. 8. Statistical analysis of trace length distributions considering all investigated sites. From top left, clockwise: trace length distribution histogram; cumulative trace length distribution; Maximum Likelihood Estimator (MLE) plots assuming a power-law distribution (right) and a lognormal distribution (left).

to be respectively parallel and perpendicular to the slopes.

Although the stress fields calculated with these methods based on radial and concentric patterns of faults, fractures and/or dikes will be examined and discussed below, it should be emphasised that the Coquand Porphyry Dike, which follows the concentric fractures trend (Fig. 3b), was emplaced around 4.7 Ma ago, while the Botro ai Marmi Granite was emplaced 5.4 Ma ago (Di Vincenzo et al., 2022). Fractures observed around the pluton top reflect the initial cooling phase of the associated metamorphic aureole; hence, fractures must pre-date dike emplacement, as suggested by the above-described time gap.

Previous authors had interpreted Porphyry Dikes Fm. emplacement as linked to horst-delimiting normal fault nucleation, as their trends are compatible (see all the dikes in Fig. 1b; Vezzoni et al., 2018; Di Vincenzo et al., 2022). In our opinion, the Coquand Dike, during emplacement, followed preferential pathways defined by the concentric fracture pattern, thus defining its geometry.

The proposed model is illustrated in Fig. 10. During *Botro ai Marmi* pluton emplacement (5.4 Ma, Di Vincenzo et al., 2022), carbonate host rocks were heated and metamorphosed, thus creating Campiglia Marittima Marble (Fig. 10a). Simultaneously, the marble developed its main schistosity, whose attitude defines at the macroscale a N–S-trending antiform fold, reflecting the pluton shape (Fig. 10a). The granitic pluton emplacement occurred at a shallow crustal level, at 3–4 km depth and 1–1.5 kbar pressure (Leoni and Tamponi, 1991; Papeschi et al., 2025).

Following the main ductile deformation event, both the granite and the marble cooled, resulting in a transition from ductile to brittle behaviour. During this time, radial and concentric fracture patterns developed (Fig. 10b). The stress field driving this deformation reflects the influence of a localised stress source, represented by the Botro ai Marmi pluton top itself, while it was probably ending its last rising event. This local stress field is limited to a slightly prolate elliptical area of influence around the pluton top, in the central part of the metamorphic aureole (Fig. 3). During this event, the maximum stress axis (σ_1) was vertical, while the intermediate (σ_2) and minimum (σ_3) stress axes were radial and concentric, respectively (Fig. 10b). σ_1 and σ_2 define the radial fracture planes that were formed. Synchronously, the σ_2 stress drop due to radial fracture formation induced a local σ_2–σ_3 inversion (e.g., Bai et al., 2002), thus defining a new σ_1–σ_2 fracture plane and enhancing concentric fracture pattern development (Fig. 3b; Fig. 10b). Accordingly, both radial and concentric fracture patterns are Mode I extensional fractures (Fossen, 2016). At this stage, new fractures started to form outside the area of influence of the pluton, with trends coherent to the imposed regional tectonic stress field (Fig. 3a).

Stress fields related to local stress sources, such as the one described above, and the associated fracture nucleation, as well as their linkage with far-field stress-related structures with increasing distance from the local stress source, have been described in the context of intrusive body emplacement (Koide and Bhattacharji, 1975), but also for diapirism phenomena involving evaporitic lithologies (Quintà et al., 2012).

Finally, the granitic pluton definitively ended its rise and stopped acting as a local stress source, leaving space for an extensional regional tectonic regime. At this stage, the main N–S to NNE–SSW- and NW–SE-trending normal faults were emplaced, thus delimiting the Campiglia Marittima horst (Fig. 10c). If the main emplacement episode of the

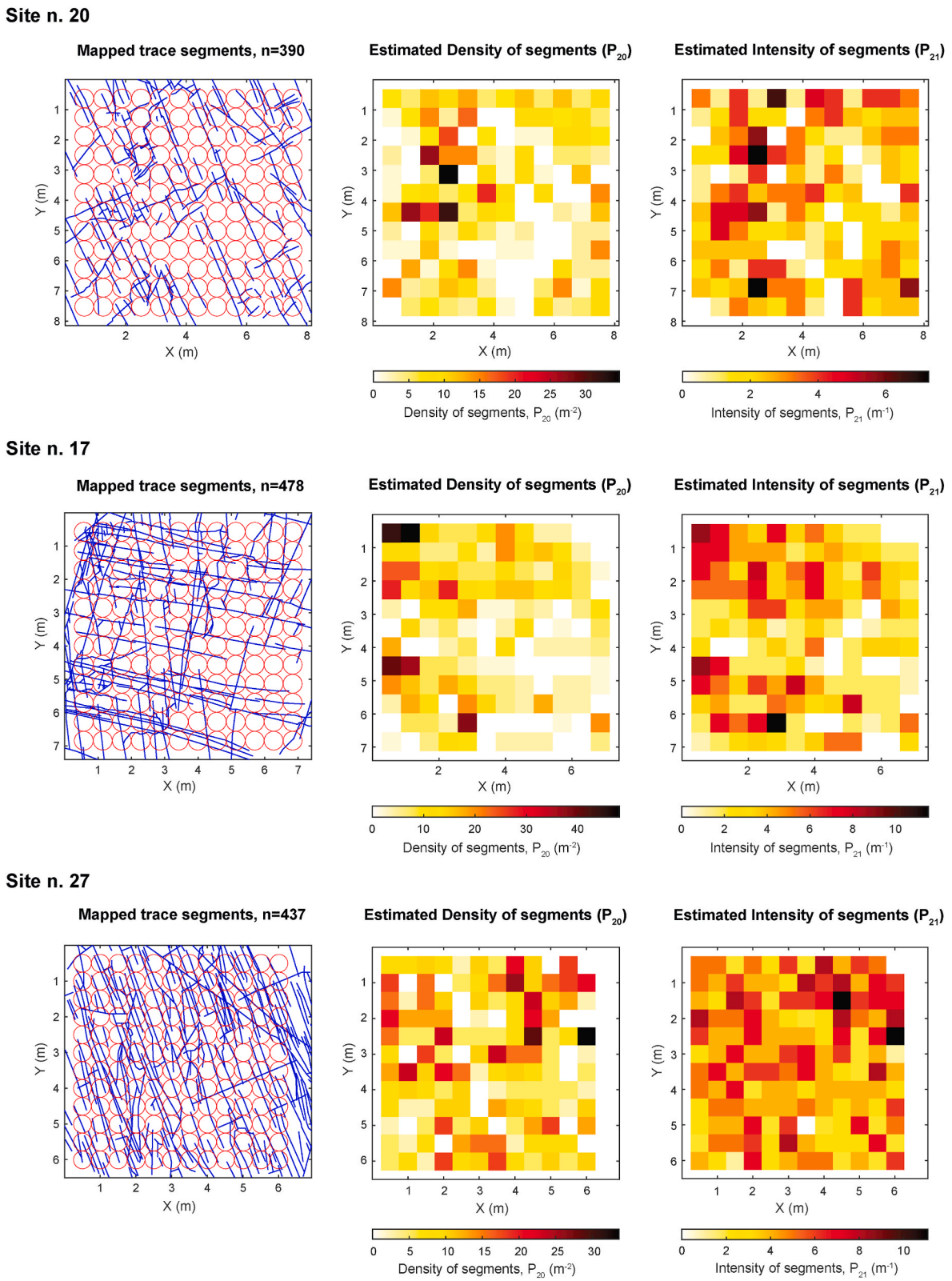

Fig. 9. Maps of estimated density (P20; middle column) and intensity (P21; right column). The left column shows scan-circle maps generated by FracPaQ2D. We imposed 12 circles per side, resulting in a circle diameter of approximately 0.6 m.

Porphyry Dikes Fm. is contemporaneous with the first fault activity, as proposed by Vezzoni et al. (2018), normal faulting should have started in this area at least at 5.1 Ma (i.e., the age of the first dikes; Di Vincenzo et al., 2022). During this stage, the Coquand Dike (4.7 Ma) was emplaced, following a preferential path influenced by the previous structures.

5.2.1. *Inferences on the regional context*

In the context of the Campiglia Marittima area, several studies focused on the skarn deposits and associated ore mineralization, as they

Table 1
Whole-map density (P20) and intensity (P21) values for each investigated site.

Site	Density (P_{20})	Intensity (P_{21})
no. 20 (Broccatello Quarry)	5.87 m^{-2}	2.44 m^{-1}
no. 17 (Calasorbi Quarry)	8.71 m^{-2}	4.55 m^{-1}
no. 27 (Pari Quarry)	9.70 m^{-2}	5.60 m^{-1}

have primary relevance for industrial and mining geology (Da Mommio et al., 2010; Vezzoni et al., 2016, 2023). However, fewer rely on the marble fracture pattern (Acocella et al., 2000; Poggetti and Tinagli, 2018).

The mechanism of the *Botro ai Marmi* granite pluton emplacement remains a matter of debate, with different models proposed over recent decades. Some authors have proposed that the Botro ai Marmi granitic body was emplaced in a newly forming releasing bend, resulting from the activity of an N-S oriented, right-lateral strike-slip fault (Acocella et al., 2000). This model has been applied to the Campiglia Marittima case, consistent with other plutons within the Tuscan Magmatic Province (Rossetti et al., 2000; Acocella and Rossetti, 2002). Other authors have argued that the granitic body rose within a full extensional tectonic setting, thereby deforming and folding the overlying limestones

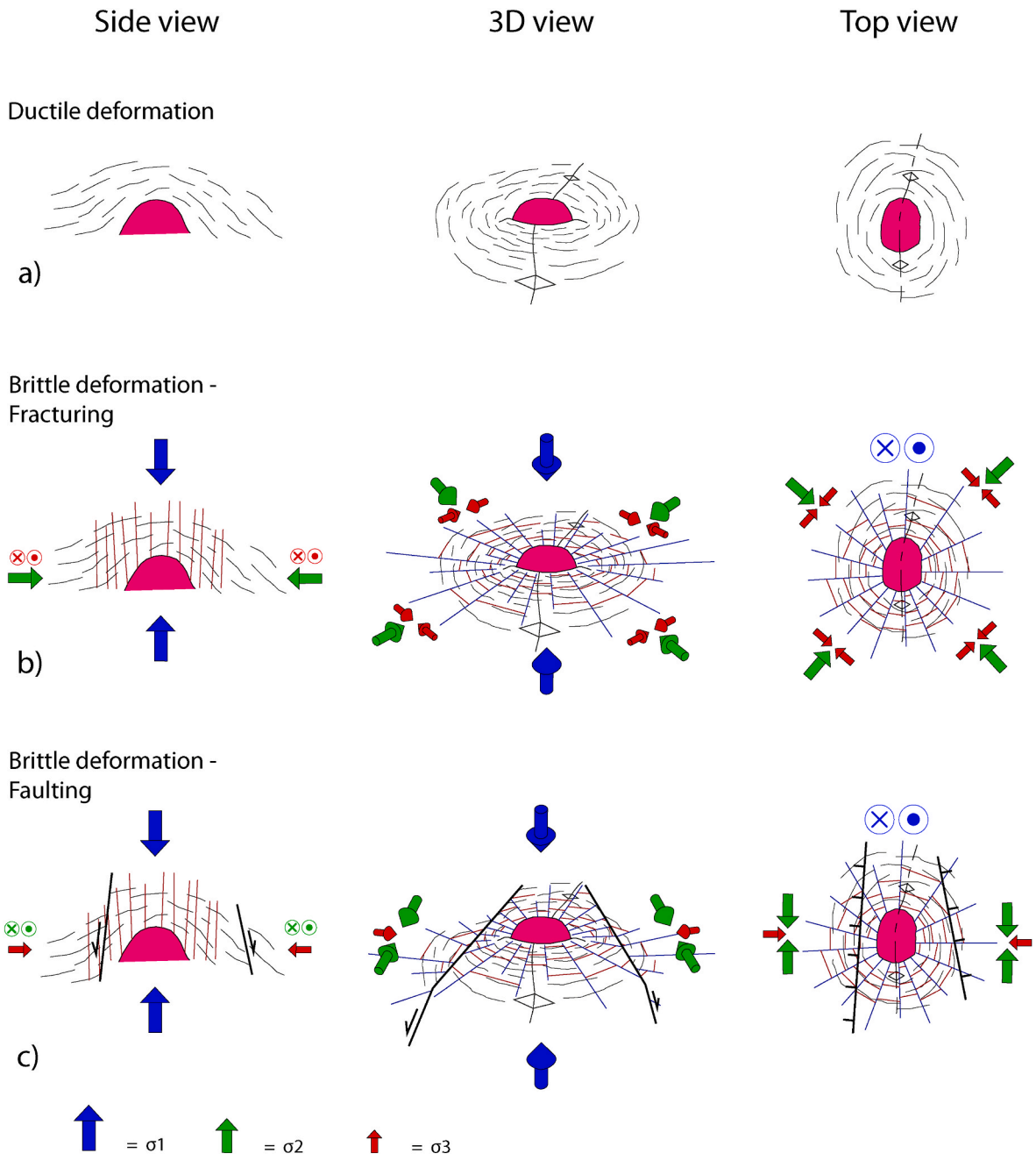

Fig. 10. Proposed model for fracture pattern evolution within pluton top-fracture related area from multiple points of view: section view (left), 3D view (middle) and top view (right). (a) Ductile deformation: Campiglia Marittima Marble are formed during *Botro ai Marmi* pluton emplacement; marble develops a main schistosity, which defines a NS-trending antiform at macroscale. (b) Brittle deformation – fracturing: latest moment of pluton rise, while both granite and marble has already cooled; radial and concentric fracture patterns occur during this step, due to local stress source constituted by the pluton top itself. (c) Brittle deformation – faulting: pluton has definitely stopped his rise at this step, and it is no more a local stress source; extensional tectonics occurs, causing normal faulting and defining the Campiglia Marittima *horst*.

(Vezzoni et al., 2018). More recently Papeschi et al. (2025) have suggested that the pluton reached the core of the developing N-S oriented anticline within a compressive stress field. In this latter view, the anticline is considered the cause, not the result, of the pluton's rise. In all these previously proposed models, magma ascent along fault planes is considered the primary mechanism that controlled the emplacement of the Botro ai Marmi Pluton.

The stress field model proposed in this paper is consistent with a full extensional tectonic setting, active at least since the latest cooling event of the Botro ai Marmi granite pluton (Fig. 10). Crucially, since the mesostructural pattern was reset by the thermometamorphism, any feature post-dating this thermal event would have recorded a regional horizontal σ_1 if a contractional or strike-slip regime were active (e.g., Hancock, 1985; Tavani et al., 2015). However, no structural evidence of such regimes, such as faults or pressure solution seams, is documented over a broad area. This lack of evidence definitively excludes both fold-and-thrust and strike-slip frameworks for the syn-to post-emplacement evolution.

6. Conclusion

This study presents an analysis of the fracture pattern within the thermo-metamorphic Campiglia Marittima Marble. To collect a large amount of data, we adopted a hybrid methodology, using both classical structural geology field surveys and the construction of Virtual Outcrop Models (VOMs) via photogrammetry using an Unmanned Aerial Vehicle (UAV). We identify radial and concentric fracture patterns radial and concentric fracture patterns within the Campiglia Marittima Marble, with respect to a centre located at the top of the Botro ai Marmi granitic pluton, which caused the marble formation. This arrangement reflects a localised stress source, consisting of the main pluton top itself, while it was ending its rise after cooling. Once formed and folded, the Campiglia Marittima Marble transitioned to a brittle deformation regime and became fractured, following a radial and concentric arrangement around the pluton top. Outside the pluton top-related fracture area, the main fracture sets are compatible with an extensional regional tectonic regime that affected the area. Within the pluton top-related area, fracture intensity is generally higher than in the rest of the metamorphic aureole. We investigated variations in fracture spacing for both radial and concentric patterns, revealing an area of lower spacing values, hence higher fracture intensity, between ~700 m and ~1.5 km distance from the pluton top.

Such a description of the fracture pattern in thermo-metamorphic marble can have several practical applications, such as in Campiglia Marittima Marble quarrying or in the study of the main fracture-associated pathways for fluid conductivity, which are the radial and concentric patterns, around the main pluton top. The latter can be useful for studying analogues geological contexts, such as the geothermal fields related to plutons present elsewhere in southern Tuscany.

CRediT authorship contribution statement

G. Risaliti: Conceptualization, Data curation, Formal analysis, Investigation, Methodology, Resources, Software, Validation, Visualization, Writing – original draft. **R.E. Rizzo:** Conceptualization, Data curation, Methodology, Resources, Software, Supervision, Validation, Visualization, Writing – original draft, Writing – review & editing. **S. Tavani:** Data curation, Methodology, Resources, Software, Validation, Visualization, Writing – original draft, Writing – review & editing. **C. Montemagni:** Conceptualization, Funding acquisition, Resources, Visualization, Writing – review & editing. **M. Coli:** Visualization, Writing – review & editing. **P. Vannucchi:** Conceptualization, Funding acquisition, Project administration, Resources, Supervision, Validation, Visualization, Writing – review & editing.

Declaration of competing interest

The authors have no conflict of interest to declare.

Acknowledgements

Funding: This work was supported by the funds from the PhD project of G. Risaliti (University of Florence). Further funds were provided by the Opera del Duomo di Firenze (COLI18FABBRICERIAOPERADUOMO, responsible P. Vannucchi), whom the authors extend their acknowledgements. The authors acknowledge the Parco Archeominerario di San Silvestro for cooperation and permission to operate in the area. Sincere acknowledgments to Dr. Niccolò Menegoni and the anonymous reviewer for their fruitful suggestions which improved the earlier version of the paper.

Appendix A. Supplementary data

Supplementary data to this article can be found online at https://doi.org/10.1016/j.jsg.2026.105759.

Data availability

Data will be made available on request.

References

Acocella, V., 2021. Volcano-Tectonic Processes, 567. Springer, Switzerland. https://doi.org/10.1007/978-3-030-65968-4.

Acocella, V., Rossetti, F., Faccenna, C., Funiciello, R., Lazzarotto, A., 2000. Strike-slip faulting and pluton emplacement in southern tuscany; the campiglia marittima case. Boll. Soc. Geol. Ital. 119 (2), 517–528.

Acocella, V., Rossetti, F., 2002. The role of extensional tectonics at different crustal levels on granite ascent and emplacement: an example from tuscany (Italy). Tectonophysics 354 (1–2), 71–83. https://doi.org/10.1016/S0040-1951(02)00290-1.

Acquater, SpA., 1994. Area Campigliese, Convenzione Ministero Industria, Commercio e Artigianato—ENI. Relazione conclusiva sui lavori svolti. In: Internal Report.

Aguilera, R., 1998. Geologic aspects of naturally fractured reservoirs. Lead. Edge 17 (12), 1667–1670. https://doi.org/10.1190/1.1437912.

Akoglu, H., 2018. User's guide to correlation coefficients. Turkish J. Emergency Med. 18 (3), 91–93. https://doi.org/10.1016/j.tjem.2018.08.001.

Bai, T., Maerten, L., Gross, M.R., Aydin, A., 2002. Orthogonal cross joints: do they imply a regional stress rotation? J. Struct. Geol. 24 (1), 77–88. https://doi.org/10.1016/S0191-8141(01)00050-5.

Bai, T., Pollard, D.D., 2000. Fracture spacing in layered rocks: a new explanation based on the stress transition. J. Struct. Geol. 22 (1), 43–57. https://doi.org/10.1016/S0191-8141(99)00137-6.

Bandini, A., Berry, P., 2013. Influence of marble's texture on its mechanical behavior. Rock Mech. Rock Eng. 46, 785–799. https://doi.org/10.1007/s00603-012-0315-1.

Barberi, F., Innocenti, F., Mazzuoli, R., 1967. Contributo alla conoscenza chimico-petrografica e magmatologica delle rocce intrusive, vulcaniche e filoniane del Campigliese (Toscana). Mem. Soc. Geol. Ital 6, 643–681.

Barboni, M., Annen, C., Schoene, B., 2015. Evaluating the construction and evolution of upper crustal magma reservoirs with coupled U/Pb zircon geochronology and thermal modeling: a case study from the mt. Capanne pluton (Elba, Italy). Earth Planet Sci. Lett. 432, 436–448. https://doi.org/10.1016/j.epsl.2015.09.043.

Barchi, M.R., 2010. The Neogene-Quaternary evolution of the Northern apennines: crustal structure, style of deformation and seismicity. In: Beltrando, M., Peccerillo, A., Mattei, M., Conticelli, S., Doglioni, C. (Eds.), Journal of the Virtual Explorer. the Geology of Italy: Tectonics and Life Along Plate Margins, 36, pp. 1–24.

Berkowitz, B., 2002. Characterizing flow and transport in fractured geological media: a review. Adv. Water Resour. 25 (8–12), 861–884. https://doi.org/10.1016/S0309-1708(02)00042-8.

Boccaletti, M., Coli, M., Decandia, F.A., Giannini, E., Lazzarotto, A., 1980. Evoluzione dell'Appennino settentrionale secondo un nuovo modello strutturale. Mem. Soc. Geol. Ital 21, 359–373, 5 ff.

Bonini, M., Sani, F., Stucchi, E.M., Moratti, G., Benvenuti, M., Menanno, G., Tanini, C., 2014. Late Miocene shortening of the Northern Apennines back-arc. J. Geodyn. 74, 1–31.

Bonnet, E., Bour, O., Odling, N.E., Davy, P., Main, I., Cowie, P., Berkowitz, B., 2001. Scaling of fracture systems in geological media. Rev. Geophys. 39 (3), 347–383.

Bratton, T., Canh, D.V., Van Que, N., Duc, N.V., Gillespie, P., Hunt, D., Li, B., Marcinew, R., Ray, S., Montaron, B., Nelson, R., Schoderbek, D., Sonneland, L., 2006. The nature of naturally fractured reservoirs. Oilfield Rev. 18 (2), 4–23.

Brogi, A., Liotta, D., Ruggieri, G., Capezzuoli, E., Meccheri, M., Dini, A., 2016. An overview on the characteristics of geothermal carbonate reservoirs in southern tuscany. Ital. J. Geosci. 135 (1), 17–29. https://doi.org/10.3301/IJG.2014.41.

Brogi, A., Liotta, D., 2008. Highly extended terrains, lateral segmentation of the substratum, and basin development: the middle-late Miocene Radicondoli Basin (inner northern Apennines, Italy). Tectonics 27 (5).
Byerlee, J., 1978. Friction of rocks. Pure Appl. Geophys. 116 (4), 615–626. https://doi.org/10.1007/BF00876528.
Cardozo, N., Allmendinger, R.W., 2013. Spherical projections with OSXStereonet. Comput. Geosci. 51, 193–205. https://doi.org/10.1016/j.cageo.2012.07.021.
Carmignani, L., Decandia, F.A., Fantozzi, P.L., Lazzarotto, A., Liotta, D., Meccheri, M., 1994. Tertiary extensional tectonics in Tuscany (northern Apennines, Italy). Tectonophysics 238 (1–4), 295–315. https://doi.org/10.1016/0040-1951(94)90061-2.
Cataldi, R., Lazzarotto, A., Muffler, P., Squarci, P., Stefani, G., 1978. Assessment of geothermal potential of central and southern Tuscany. Geothermics 7 (2–4), 91–131. https://doi.org/10.1016/0375-6505(78)90003-2.
Cavari, F., Droghini, F., Giamello, M., Lazzarini, L., Mascione, C., 2012. The white marble quarries of Campiglia Marittima (Livorno, Italy) and the provenance of marble artefacts from Populonia'. Interdisciplinary Studies on Ancient Stone. ASMOSIA IX, 390–400.
Cerrina Feroni, A., Fedeli, A., Martinelli, P., Ungari, A., Baldacci, F., Masetti, G., 2007a. Carta geologica Della Toscana Alla Scala 1:10.000, Sezione 305080. Sassetta. CNR – Istituto di Geoscienze e Georisorse, Regione Toscana.
Cerrina Feroni, A., Fedeli, A., Ungari, A., Catanzariti, R., Masetti, G., 2007b. Carta geologica Della Toscana Alla Scala 1:10.000, Sezione 305120, Campiglia Marittima. CNR – Istituto di Geoscienze e Georisorse, Regione Toscana.
Chadwick Jr, W.W., Dieterich, J.H., 1995. Mechanical modeling of circumferential and radial dike intrusion on Galapagos volcanoes. J. Volcanol. Geoth. Res. 66 (1–4), 37–52. https://doi.org/10.1016/0377-0273(94)00060-T.
Conti, P., Cornamusini, G., Carmignani, L., 2020. An outline of the geology of the Northern Apennines (Italy), with geological map at 1: 250,000 scale. Ital. J. Geosci. 139 (2), 149–194.
Cosgrove, J.W., Hudson, J.A., 2016. Structural Geology and Rock Engineering. World Scientific Publishing Company. https://doi.org/10.1142/p1084.
Costantini, A., Lazzarotto, A., Maccantelli, M., Mazzanti, R., Sandrelli, F., Tavarnelli, E., Elter, F.M., 1993. Geologia della provincia di Livorno a sud del Fiume Cecina. Quad Mus Stor Nat di Livorno 13 (Suppl. 2), 1–164.
Da Mommio, A., Iaccarino, S., Vezzoni, S., Dini, A., Rocchi, S., Brocchini, D., Guideri, S., Sbrilli, L., 2010. Valorizzazione del geosito «sezione Coquand», Miniera del Temperino (Parco Archeominerario di San Silvestro, Campiglia Marittima). Atti Della Società Toscana Di Scienze Naturali Residente In Pisa. Memorie. Serie A 115, 55–72.
Davis, N.E., Kronenberg, A.K., Newman, J., 2008. Plasticity and diffusion creep of dolomite. Tectonophysics 456 (3–4), 127–146.
Delaney, P.T., Pollard, D.D., Ziony, J.I., McKee, E.H., 1986. Field relations between dikes and joints: emplacement processes and paleostress analysis. J. Geophys. Res. Solid Earth 91 (B5), 4920–4938. https://doi.org/10.1029/JB091iB05p04920.
Dershowitz, W.S., Einstein, H.H., 1988. Characterizing rock joint geometry with joint system models. Rock Mech. Rock Eng. 21 (1), 21–51. https://doi.org/10.1007/BF01019674.
Dershowitz, W.S., Herda, H.H., 1992. Interpretation of fracture spacing and intensity. In: ARMA US Rock mechanics/geomechanics Symposium. ARMA-92. ARMA.
Di Vincenzo, G., Vezzoni, S., Dini, A., Rocchi, S., 2022. Timescale of a magmatic-hydrothermal system revealed by 40Ar–39Ar geochronology: the Mio-Pliocene Campiglia Marittima system (Tuscany, Italy). Sci. Rep. 12 (1), 7128.
Fossen, H., 2016. Structural Geology. Cambridge university press.
Franzini, M., Lezzerini, M., Origlia, F., 2010. Marbles from the Campiglia marittima area (Tuscany, Italy). Eur. J. Mineral 22 (6), 881–893. https://doi.org/10.1127/0935-1221/2010/0022-2056.
Giannini, E., 1955. Geologia Dei Monti Di Campiglia Marittima (Livorno). Pacini Mariotti.
Gratier, J.P., Gueydan, F., 2007. Effect of fracturing and fluid–rock interaction on seismic cycles. Tectonic Faults: Agents Of Change A Dynamic Earth 95, 319–356. https://doi.org/10.7551/mitpress/6703.003.0014.
Hancock, P.L., 1985. Brittle microtectonics: principles and practice. J. Struct. Geol. 7 (3–4), 437–457. https://doi.org/10.1016/0191-8141(85)90048-3.
Hancock, P.L., Engelder, T., 1989. Neotectonic joints. Geol. Soc. Am. Bull. 101 (10), 1197–1208. https://doi.org/10.1130/0016-7606(1989)101<1197:NJ>2.3.CO;2. GSA Bulletin (1989) 101 (10): 1197–1208.
Harbord, C., Brantut, N., Wallis, D., 2023. Grain-size effects during semi-brittle flow of calcite rocks. J. Geophys. Res. Solid Earth 128. https://doi.org/10.1029/2023JB026458 e2023JB026458.
Healy, D., Rizzo, R.E., Cornwell, D.G., Farrell, N.J., Watkins, H., Timms, N.E., Gomez-Rivas, E., Smith, M., 2017. FracPaQ: a MATLAB™ toolbox for the quantification of fracture patterns. J. Struct. Geol. 95, 1–16. https://doi.org/10.1016/j.jsg.2016.12.003.
Jolivet, L., Faccenna, C., D'Agostino, N., Fournier, M., Worrall, D., 1999. The kinematics of back-arc basins, examples from the Tyrrhenian, Aegean and Japan Seas. Geological Society, London, Special Publications 164 (1), 21–53. https://doi.org/10.1144/GSL.SP.1999.164.01.04.
Koide, H., Bhattacharji, S., 1975. Formation of fractures around magmatic intrusions and their role in ore localization. Econ. Geol. 70 (4), 781–799. https://doi.org/10.2113/gsecongeo.70.4.781.
Lamarche, J., Lavenu, A.P., Gauthier, B.D., Guglielmi, Y., Jayet, O., 2012. Relationships between fracture patterns, geodynamics and mechanical stratigraphy in Carbonates (South-East Basin, France). Tectonophysics 581, 231–245. https://doi.org/10.1016/j.tecto.2012.06.042.
Lavenu, A.P., Lamarche, J., Gallois, A., Gauthier, B.D., 2013. Tectonic versus diagenetic origin of fractures in a naturally fractured carbonate reservoir analog (Nerthe anticline, southeastern France). AAPG Bull. 97 (12), 2207–2232. https://doi.org/10.1306/04041312225.
Lavenu, A.P., Lamarche, J., 2018. What controls diffuse fractures in platform carbonates? Insights from Provence (France) and Apulia (Italy). J. Struct. Geol. 108, 94–107. https://doi.org/10.1016/j.jsg.2017.05.011.
Leoni, L., Tamponi, M., 1991. Thermometamorphism in the Campiglia Marittima aureole (Southern Tuscany, Italy). Neues Jahrbuch fur Mineralogie Monatshefte 4, 145–157.
Lezzerini, M., Civita, J., Aquino, A., Pagnotta, S., 2021. Marbles from castagneto carducci area (Tuscany, Italy). IOP Conf. Ser. Earth Environ. Sci. 906 (1), 012122. IOP Publishing.
Liotta, D., Brogi, A., Ruggieri, G., Zucchi, M., 2021. Fossil vs. active geothermal systems: a field and laboratory method to disclose the relationships between geothermal fluid flow and geological structures at depth. Energies 14 (4), 933. https://doi.org/10.3390/en14040933.
Malinverno, A., Ryan, W.B., 1986. Extension in the tyrrhenian sea and shortening in the Apennines as result of arc migration driven by sinking of the lithosphere. Tectonics 5 (2), 227–245. https://doi.org/10.1029/TC005i002p00227.
Mancktelow, N.S., 2009. Fracture and flow in natural rock deformation. Trab. Geol. 29.
Martel, S.J., Bergbauer, S., 1997. Testing a thermal-stress origin of fractures in a pluton. Int. J. Rock Mech. Min. Sci. 34 (3–4). https://doi.org/10.1016/S1365-1609(97)00142-1, 191-e1.
Menegoni, N., Giordan, D., Perotti, C., Tannant, D.D., 2019. Detection and geometric characterization of rock mass discontinuities using a 3D high-resolution digital outcrop model generated from RPAS imagery–Ormea rock slope, Italy. Eng. Geol. 252, 145–163. https://doi.org/10.1016/j.enggeo.2019.02.028.
Molli, G., 2008. Northern apennine–Corsica orogenic system: an updated overview. https://doi.org/10.1144/SP298.19.
Morgan, S.S., 1998. Pluton Emplacement, Aureole Deformation and Metamorphism, and Regional Deformation Within the Central White-Inyo Range, Eastern California. Virginia Polytechnic Institute and State University. http://hdl.handle.net/10919/39677.
Muller, O.H., Pollard, D.D., 1977. The stress state near Spanish peaks, Colorado determined from a dike pattern. Pure Appl. Geophys. 115 (1), 69–86. https://doi.org/10.1007/BF01637098.
Narr, W., Suppe, J., 1991. Joint spacing in sedimentary rocks. J. Struct. Geol. 13 (9), 1037–1048. https://doi.org/10.1016/0191-8141(91)90055-N.
Odé, H., 1957. Mechanical analysis of the dike pattern of the Spanish peaks area, Colorado. Geol. Soc. Am. Bull. 68 (5), 567–576. https://doi.org/10.1130/0016-7606(1957)68[567:MAOTDP]2.0.CO;2.
Papeschi, S., Bonini, M., Lanari, R., Del Ventisette, C., Montanari, D., 2025. Growth of a magma-filled antiform from granite emplacement to post-intrusive cooling: the campiglia marittima study case (Northern Apennines, Italy). Lithos 504, 108053. https://doi.org/10.1016/j.lithos.2025.108053.
Passchier, C.W., Trouw, R.A., 2005. Microtectonics. Springer Berlin Heidelberg, Berlin, Heidelberg. https://doi.org/10.1007/3-540-29359-0.
Peacock, D.C.P., Sanderson, D.J., Rotevatn, A., 2018. Relationships between fractures. J. Struct. Geol. 106, 41–53. https://doi.org/10.1016/j.jsg.2017.11.010.
Pearson, K., 1895. VII. Note on regression and inheritance in the case of two parents. Proc. Roy. Soc. Lond. 58 (347–352), 240–242. https://doi.org/10.1098/rspl.1895.0041.
Peccerillo, A., 2017. The tuscany Province. In: Cenozoic Volcanism in the Tyrrhenian Sea Region. Advances in Volcanology. Springer, Cham. https://doi.org/10.1007/978-3-319-42491-0_2.
Pix4D, 2025. *PIX4Dmapper* (Version 4.7.3). Pix4D SA. Retrieved from. www.pix4d.com/product/pix4dmapper-photogrammetry-software.
Poggetti, E., Tinagli, L., 2018. Analisi Speditiva Del Quadro Fessurativo Caratterizzante Gli Ambienti Sotterranei Della "Ricerca Buca Del Serpente" (Campiglia Marittima, Toscana).
Pollard, D.D., Aydin, A., 1988. Progress in understanding jointing over the past century. Geol. Soc. Am. Bull. 100 (8), 1181–1204. https://doi.org/10.1130/0016-7606(1988)100%3C1181:PIUJOT%3E2.3.CO;2.
Quintà, A., Tavani, S., Roca, E., 2012. Fracture pattern analysis as a tool for constraining the interaction between regional and diapir-related stress fields: Poza de la Sal Diapir (Basque Pyrenees, Spain). https://doi.org/10.1144/SP363.25.
Rawnsley, K.D., Rives, T., Petti, J.P., Hencher, S.R., Lumsden, A.C., 1992. Joint development in perturbed stress fields near faults. J. Struct. Geol. 14 (8–9), 939–951. https://doi.org/10.1016/0191-8141(92)90025-R.
Risaliti, G., Mancini, S., Coli, M., 2026. The marble of campiglia: an historical cultural Heritage ornamental stone from tuscany, Italy. Heritage 9 (5), 190. https://doi.org/10.3390/heritage9050190.
Rizzo, R.E., Healy, D., De Siena, L., 2017. Benefits of maximum likelihood estimators for fracture attribute analysis: implications for permeability and up-scaling. J. Struct. Geol. 95, 17–31. https://doi.org/10.1016/j.jsg.2016.12.005.
Rossetti, F., Faccenna, C., Acocella, V., Funiciello, R., Jolivet, L., Salvini, F., 2000. Pluton emplacement in the northern Tyrrhenian area, Italy. Geological Society, London, Special Publications 174 (1), 55–77. https://doi.org/10.1144/GSL.SP.1999.174.01.04.
Schmid, S.M., 1982. Microfabric studies as indicators of deformation mechanisms and flow laws operative. In: Hsu, K.J. (Ed.), Mountain Building Processes. Academic Press, London, pp. 95–110.
Segall, P., 1984. Formation and growth of extensional fracture sets. Geol. Soc. Am. Bull. 95 (4), 454–462. https://doi.org/10.1130/0016-7606(1984)95%3C454:FAGOEF%3E2.0.CO;2.

Segall, P., Pollard, D.D., 1983. Nucleation and growth of strike slip faults in granite. J. Geophys. Res. Solid Earth 88 (B1), 555–568. https://doi.org/10.1029/JB088iB01p00555.

Serri, G., Innocenti, F., Manetti, P., 2001. Magmatism from Mesozoic to present: petrogenesis, time-space distribution and geodynamic implications. In: Anatomy of an Orogen: the Apennines and Adjacent Mediterranean Basins. Springer Netherlands, Dordrecht, pp. 77–103. https://doi.org/10.1007/978-94-015-9829-3_8.

Spence, G.H., Couples, G.D., Bevan, T.G., Aguilera, R., Cosgrove, J.W., Daniel, J.M., Redfern, J., 2014. Advances in the study of naturally fractured hydrocarbon reservoirs: a broad integrated interdisciplinary applied topic. https://doi.org/10.1144/SP374.19.

Tavani, S., Arbues, P., Snidero, M., Carrera, N., Muñoz, J.A., 2011. Open Plot Project: an open-source toolkit for 3-D structural data analysis. Solid Earth 2 (1), 53–63.

Tavani, S., Storti, F., Lacombe, O., Corradetti, A., Muñoz, J.A., Mazzoli, S., 2015. A review of deformation pattern templates in foreland basin systems and fold-and-thrust belts: implications for the state of stress in the frontal regions of thrust wedges. Earth Sci. Rev. 141, 82–104. https://doi.org/10.1016/j.earscirev.2014.11.013.

Terzaghi, R.D., 1965. Sources of error in joint surveys. Geotechnique 15 (3), 287–304. https://doi.org/10.1680/geot.1965.15.3.287.

Tóth, E., Hrabovszki, E., Schubert, F., Toth, T.M., 2022. Discrete fracture network (DFN) modelling of a high-level radioactive waste repository host rock and the effects on its hydrogeological behaviour. J. Struct. Geol. 156, 104556. https://doi.org/10.1016/j.jsg.2022.104556.

Vezzoni, S., Dini, A., Rocchi, S., 2016. Reverse telescoping in a distal skarn system (Campiglia Marittima, Italy). Ore Geol. Rev. 77, 176–193. https://doi.org/10.1016/j.oregeorev.2016.03.001.

Vezzoni, S., Rocchi, S., Dini, A., 2018. Lateral extrusion of a thermally weakened pluton overburden (Campiglia Marittima, Tuscany). Int. J. Earth Sci. 107, 1343–1355. https://doi.org/10.1007/s00531-017-1539-9.

Vezzoni, S., Rocchi, S., Dini, A., 2023. Campiglia marittima skarn (Tuscany): a challenging example for the evolution of skarn-forming models. Minerals 13 (4), 482. https://doi.org/10.3390/min13040482.

Vigneresse, J.L., Tikoff, B., Améglio, L., 1999. Modification of the regional stress field by magma intrusion and formation of tabular granitic plutons. Tectonophysics 302 (3–4), 203–224. https://doi.org/10.1016/S0040-1951(98)00285-6.

Walter, B., Géraud, Y., Diraison, M., Bertrand, L., Le Garzic, E., Oliot, E., Perry, G., 2013. Insight of syn-tectonic crystalline reservoirs. Effect of inherited structures on fracture networks (eg Elba Island). In: Second EAGE Workshop on Naturally Fractured Reservoirs. European Association of Geoscientists & Engineers, p. 371. https://doi.org/10.3997/2214-4609.20132035.

Yue, L., Li, W., Liu, Y., Li, S., Wang, J., 2024. A review of mechanical deformation and seepage mechanism of rock with filled joints. Deep Underground Science and Engineering 3 (4), 439–466. https://doi.org/10.1002/dug2.12126.